Mechanics of Materials 123 (2018) 30–42

Contents lists available at ScienceDirect

Mechanics of Materials

journal homepage: www.elsevier.com/locate/mechmat

Research paper

Dynamic tension of ductile polymers: Experimentation and modelling

S. Tzibula[a,b], Z. Lovinger[a,b,*], D. Rittel[a]

[a] Technion –Faculty of Mechanical Engineering, Technion, Haifa, 32000, Israel
[b] RAFAEL, P. O. B 2250, 21031, Israel

ABSTRACT

Two main problems are recurrently mentioned when performing dynamic tension tests of polymers: The weak transmitted signal, often close to the level of the signal noise, and the (in)ability to achieve dynamic force equilibrium. In this work, we investigated the dynamic tensile response of commercial polycarbonate (PC) using the Kolsky-Bar apparatus and digital image correlation (DIC). We conducted 2D numerical simulations to explore the sensitivities of the experimental apparatus and to simulate the dynamic tests. By specifically focusing on the material behavior within the dynamically evolving neck, calibration of a stress strain curve was achieved in combination of numerical modeling. We introduce a "4-point model" that can successfully predict the location of the neck and the strain distribution along the specimens. The static tensile, dynamic tensile and dynamic compressive behavior of commercial PC are compared, and our analysis suggests a strong correlation between the three. This observation could facilitate the measurement of the dynamic tensile strength of polymers – to be possibly extracted from dynamic compression or static tension measurements only.

1. Introduction

The behavior of glassy polymers at high strain rates is of growing interest for different industries that use polymers as a major structural material, for example crashworthiness and lightweight armor applications.

For design purposes, there is a need to determine the dynamic behavior of the material under both compression and tension. One of the most common experimental techniques for measuring the dynamic behavior of materials at high strain rates is the Kolsky-Bar (also known as the Split-Hopkinson Bar) apparatus (Kolsky, 1949). While the testing of polymers in compression is relatively well documented (Walley and Field, 1994; Mulliken and Boyce, 2004; Richeton et al., 2006), tensile testing is very challenging from an experimental point of view. When compared with metals, polymers have a low mechanical impedance and yield stress, so that the transmitted signal can be very weak and buried into the electrical noise. The weak transmitted signal and the ability to reach good equilibrium within the specimen are the two main challenges in dynamic tensile testing of polymers.

The impedance mismatch problem has led various researchers to adopt lower impedance pressure bars, specifically titanium (Gray et al., 1997), aluminum (Nie et al., 2009), magnesium (Subhash et al., 2006), and, finally, polymer pressure bars (Wang et al., 1994; Zhao and Gary, 1995; Sawas et al., 1998). While the lower inherent impedance of polymers pressure bars offers positive attributes to Kolsky-Bar testing of soft materials, their use introduces several complications due to their low strength when mounting threaded joints to the specimen and due to their low melting point when testing at elevated temperatures. Another issue is that of the stress wave propagation into viscoelastic bars that may necessitate additional corrections to those commonly performed in Kolsky bar testing (Zhao and Gary, 1995; Bacon, 1998; Benatar et al., 2003).

The low impedance metallic bars are a convenient compromise between the low impedance and sufficient strength. Likewise, another approach to mechanically (geometrically) amplify the transmitted signal consists of using a hollow transmitted bar (Chen and Lu, 2002).

The seminal work of Kolsky (1949) on polymers should be mentioned here, in which he determined the importance of using thin specimens to reduce the time a specimen takes to reach a state of uniform uniaxial stress, followed by 2–3 reverberations through the specimen thickness. His studies demonstrated that thin samples were critical when studying the high rate constitutive response of plastics or the assumption that the pressure on both sides of the specimen is equal is no longer valid.

Equilibrium within the tested specimen is required to ensure uniform stress, fulfilling the basic assumptions of the Kolsky bar analysis, allowing to extract the stress-strain curve from the test. Additional considerations of dynamic load equilibrium and specimen dimensions can be found in the works of Koubaa et al. (2011) and Rotbaum and Rittel (2014). The latter addressed the actual question of the optimized

* Corresponding author.
E-mail address: lovinger@caltech.edu (Z. Lovinger).

https://doi.org/10.1016/j.mechmat.2018.04.014
Received 12 January 2018; Received in revised form 10 April 2018; Accepted 17 April 2018
Available online 20 April 2018

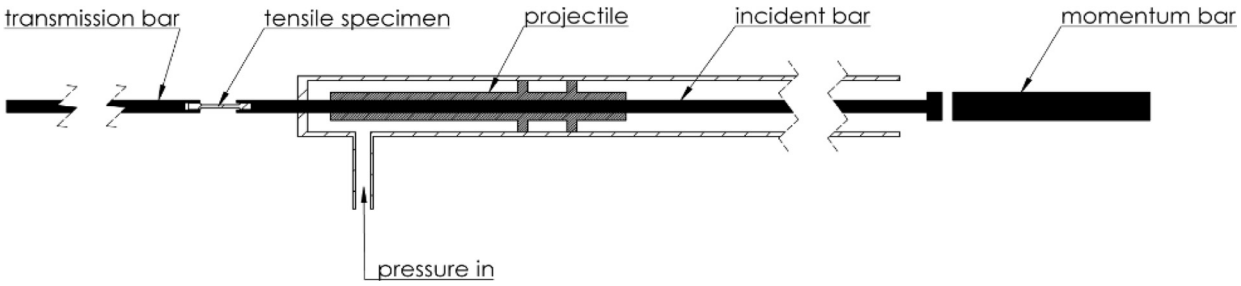

Fig. 1. Schematic representation of the Kolsky-Bar apparatus.

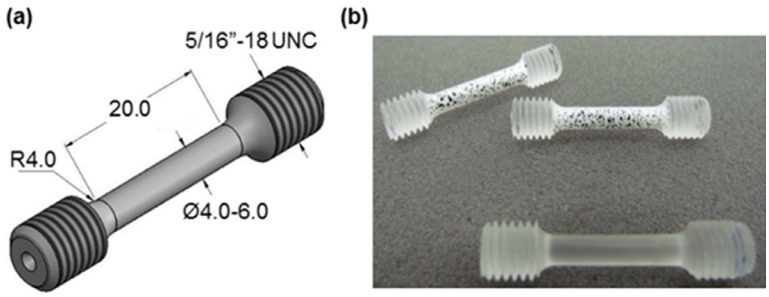

Fig. 2. Dog Bone specimen: (a) Specimen's geometry. (b) Specimen's surface painting.

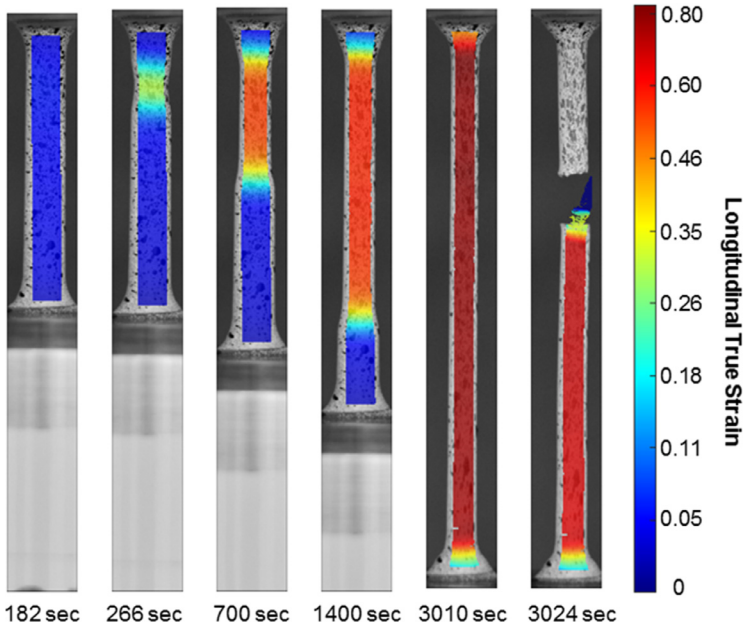

Fig. 3. DIC images for the PC-S01 quasi-static tensile test.

specimen's length in such tests. They showed, using numerical simulations, that load equilibrium does not necessarily express a uniform state of stress and strain for short specimens. Furthermore, these authors reported the counterintuitive result that long specimens are favorable for dynamic testing, enabling a more uniform stress and strain distribution along the specimen's gauge length, which in turns increases the reliability of the determined stress strain curve.

Another way to achieve stress equilibrium at low strains is to increase the rise time of the incident loading pulse with a pulse shaper (Nie et al., 2009; Chen and Lu, 2002; Sarva and Boyce, 2007; Gerlach et al., 2011). While a longer rise time increases the ability to reach equilibrium in the specimen, it lowers the effective strain rate. Furthermore, the use of pulse shapers remains a matter of experience via trial and error to determine the appropriate pulse shaping material and its thickness.

An additional way to overcome the difficulties of equilibrium in such tests is to examine the *actual* dynamic evolution of stress and strain in the specimen. This can be done by continuous strain measurements of the specimen during its loading, using Digital Image Correlation (DIC) for instance. Foster et al., 2015) recently analyzed the stress strain curve of PC by combining high speed photography with DIC to determine the specimen's evolving strain, and a piezoelectric load cell instead of the transmitted bar to measure the force transferred to the specimen. The stress strain behavior was directly extracted from these measurements. Foster et al. (2015) further implemented in their experimental system a place-on grip to bypass the difficulties of the screw mounting of the soft polymeric specimen to the metallic bars.

However, the vast majority of the studies in the field carefully avoid drawing any conclusions from the onset of tensile necking and beyond. A few of them eventually apply empirical or analytical corrections that

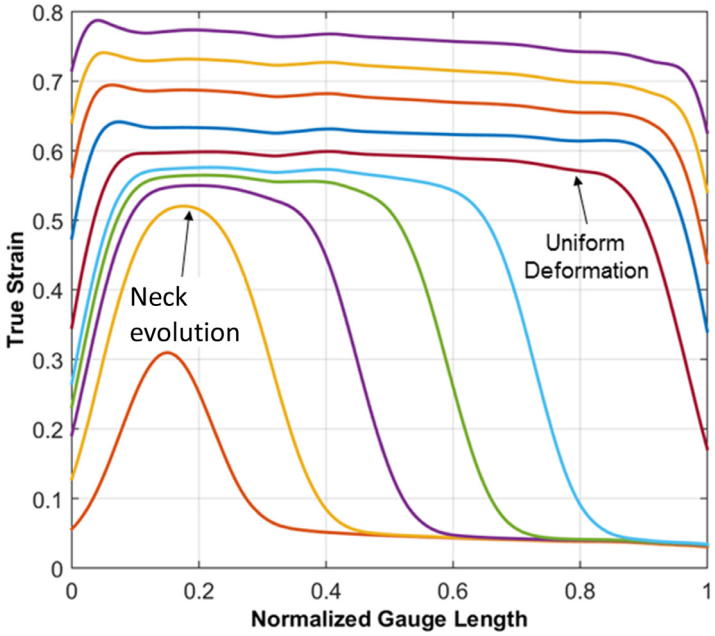

Fig. 4. Longitudinal true strain evolution along the PC specimen: normalized gauge length (Time steps every 280 seconds).

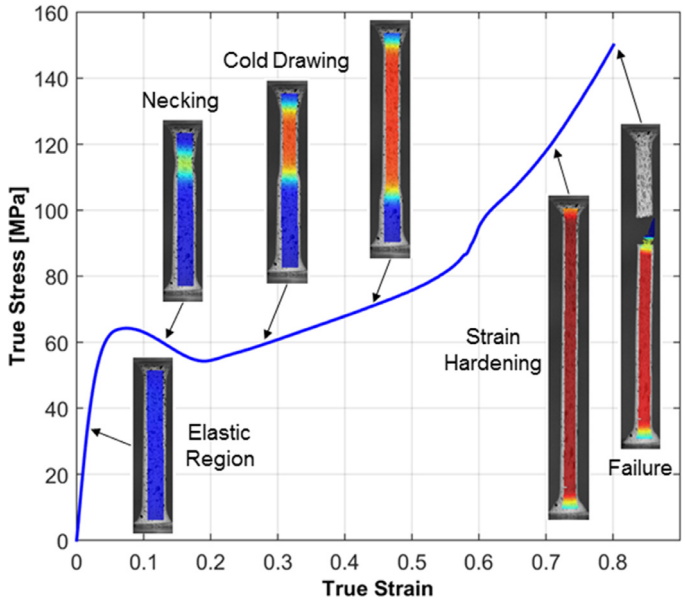

Fig. 5. True quasi-static tensile stress-strain curve for PC. Strain measured at interest zone around eventual failure point.

require additional experimental information (Bridgman, 1952; Mirone, 2004; Mirone, 2013), none of which applied to polymer testing so far. One should mention here the work of Cao et al. (2014) who performed dynamic tensile experiments using special semiconductor strain gages to enhance the transmitted signal and modeled the behavior of PC. However, these authors did not address the neck formation nor its location on the specimen's gauge length, limited also to relatively low strains.

This study seeks to characterize the dynamic tensile behavior of PC, based on a standard tensile Kolsky bar apparatus. This work presents an Inverse Finite Element method to analyze the behavior of PC in the dynamically loaded specimen, using DIC and focusing on the analysis of the large strains, *precisely in the evolving neck*. A phenomenological "4 point" material model is presented, following the dominant physics, ruling the PC tensile behavior, an attempt to reproduce the post yield behavior in the tests. Further experimental work in quasi-static tension and dynamic compression were conducted for comparison with the dynamic tension results and analysis.

2. Experimental testing

2.1. Dynamic tensile testing

2.1.1. Kolsky-Bar apparatus

The dynamic tensile system used in this work is a 12.7 mm diameter Kolsky apparatus (Kolsky, 1949; Harding et al., 1960) made of Aluminum 7075-T6 bars, which were loaded at the end of the incident bar with a 400 mm long tubular projectile made of the same material. Incident and transmitted bars are 2.4 m and 1.4 m long. A momentum trap was used, brought initially in contact with the loaded flange of the incident bar, having the same cross section as the projectile bar, as shown in Fig. 1. Strain gauges were attached on the incident and

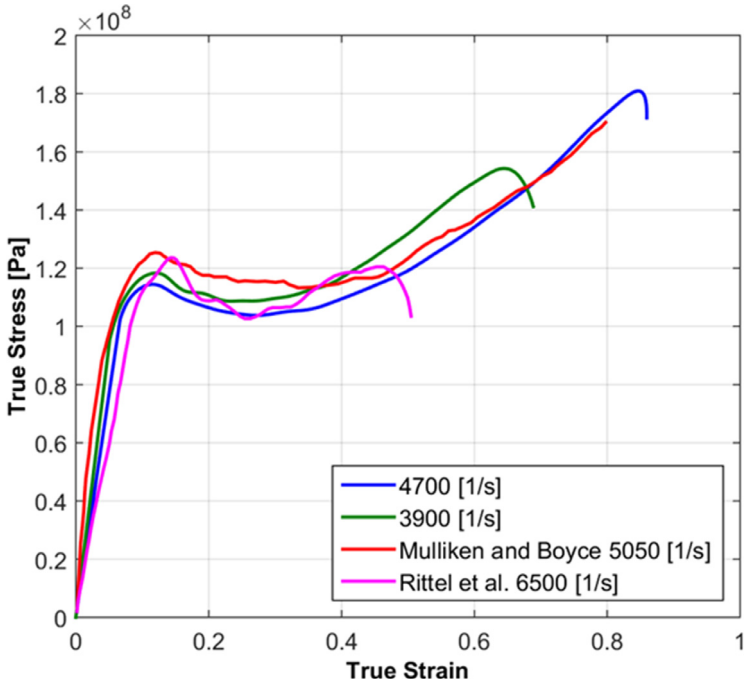

Fig. 6. True stress-strain curves for dynamic compression PC's specimens – comparison with other results in the literature.

Table 1
Summary of the dynamic tension experiments with PC specimen.

Test Serial No.	Gauge Diameter [mm]	Gauge Length [mm]	Strain Rate [s^{-1}]
L6_15_1	6	15	1100
L6_15_2	6	15	1300
L5_15_1	5	15	1000
L5_15_2	5	15	1100
L4_20_1	4	20	1050
L4_20_2	4	20	1050
L4_20_3	4	20	1070
L4_20_4	4	20	1100
L4_20_5	4	20	1250
L4_20_6	4	20	1150

transmitted bars to measure the wave signals, before and after the interaction with the specimen.

2.1.2. Specimen material and geometry

The tested material was Polycarbonate manufactured by Ensinger supplied as a 10.0 mm diameter bar, tested in the as-received condition. The specimen was machined to a cylindrical axisymmetric "Dog Bone" shaped sample with threaded ends. Specimen's dimensions were determined based on the ASTM E8M standard (ASTM Int., 2016): The diameters of the cross section varied from 4mm-6 mm, and the gauge length was 15–20 mm. Relating to the above explained trade-off between a shorter specimen that allows reaching earlier equilibrium, and a longer specimen, which introduces a much more uniform stress and strain distribution along the specimen (Koubaa et al., 2011; Rotbaum and Rittel, 2014), the range of dimensions we chose for this research was found to be a good compromise between the two, as will be shown later in the numerical analysis. For DIC application, the specimens were spray painted using an alcohol based black ink. Specimen's geometry and the surface painting are shown in Fig. 2.

2.1.3. Digital image correlation (DIC)

In order to measure the large evolving strains, the Ncorr open source 2D DIC code (Blaber et al., 2015) was used to analyze the pictures extracted from the ultrahigh speed Kirana camera using 500,000 frames per second. The high speed camera was synchronized with the incident bar signals to capture the evolution of the specimens and neck inception, in order to separate the post necking process from the uniform deformation phase. Strains were extracted along the centerline of the specimen to avoid errors in averaging a 2D strain data field over the 3D curved specimen surface.

2.2. Quasi-static tensile testing

Quasi-static tensile tests were carried out using Instron electromechanical screw driven machine model 4400. During the tests a 5 KN load cell measured the load applied to the specimen and a DSLR Nikon D700 camera was used to film the specimen at a rate of one frame every 14 s. All experiments were performed with a prescribed crosshead velocity of 0.5 mm/min.

The quasi-static tensile testing used the same "Dog Bone" specimens as for the dynamic tests, showed in Fig. 2.

2.3. Dynamic compression testing

Dynamic compression tests were carried out on a 19.05 mm diameter Kolsky apparatus made of Maraging C300 bars, which were loaded at the end of the incident bar with a 280 mm long projectile made of the same material. Specimen dimensions were Ø10 × 5 mm. We note that *in compression*, due to the significant transmitted signal, the impedance mismatch with the bars played no role in the material property analysis.

3. Results

As explained above, although the main goal of the research was to measure the dynamic behavior of PC in tension, we tested the material in dynamic compression and quasi-static tension as well. The results of these more standard tests are presented first, allowing the comparative discussion in the sequel, when dynamic test results are analyzed.

3.1. Quasi-static tensile tests

The elongation behavior of the material during the quasi-static

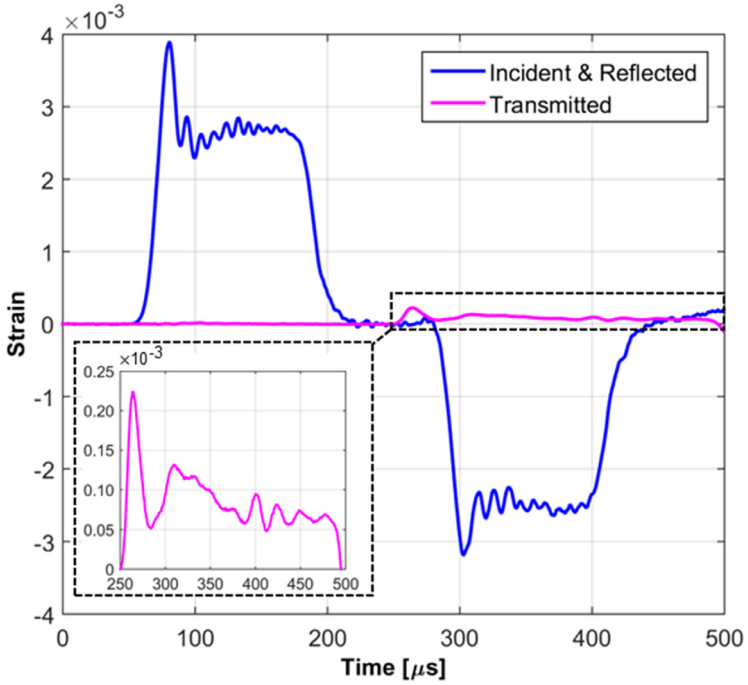

Fig. 7. Measured strain signals in test L4_20_5, the inset is a zoomed view of the transmitted signal.

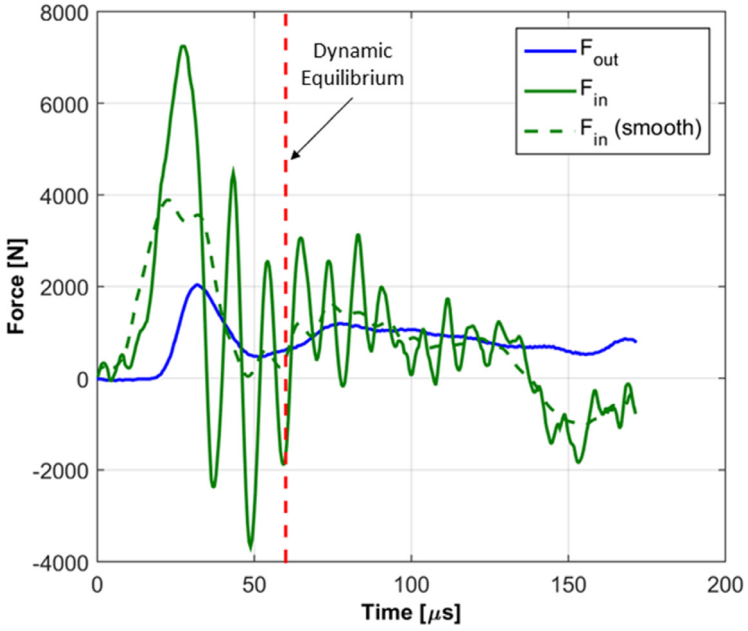

Fig. 8. Dynamic force equilibrium during dynamic tensile test L4_20_5 – original and filtered signals.

tensile test is shown in the sequential pictures in Fig. 3. Typical for ductile polymers, the specimen initially develops a neck followed by a process similar to cold drawing, yielding the entire gauge section. After the whole specimen reaches a uniform strain, a hardening phase is evident with a significant increase in the measured force, up to the occurrence of fracture.

Using mechanical or laser extensometers results in averaging the strain over an area of the specimen which not necessarily includes the initial neck. The DIC allows us to use the strain measurements at the specific region which is initially necked, in each test, therefore, obtaining an accurate stress-strain behavior which represents the real material behavior in the post yield stage. Notice that the point where the specimen initially necked is not necessarily the one where the specimen eventually fails at the end of the experiment. The strain history we used to extract the stress-strain curve was measured in the middle of the initial neck.

In Fig. 4 the distribution of the longitudinal true strain is shown along the specimen's gauge length. Each plot, moving from the bottom to the top represents a specific time during the test sampled every 280 s. The extent of the necked region is clearly shown, until the whole gauge length deforms uniformly.

A true stress-strain curve of one of the tests is shown in Fig. 5. The following regions of behavior can be observed along the curve: An elastic region, the yielding, observed at ~65 MPa, the softening during the necking, the cold drawing stage characterized by strain hardening and the final stage of additional hardening after the full yield of the

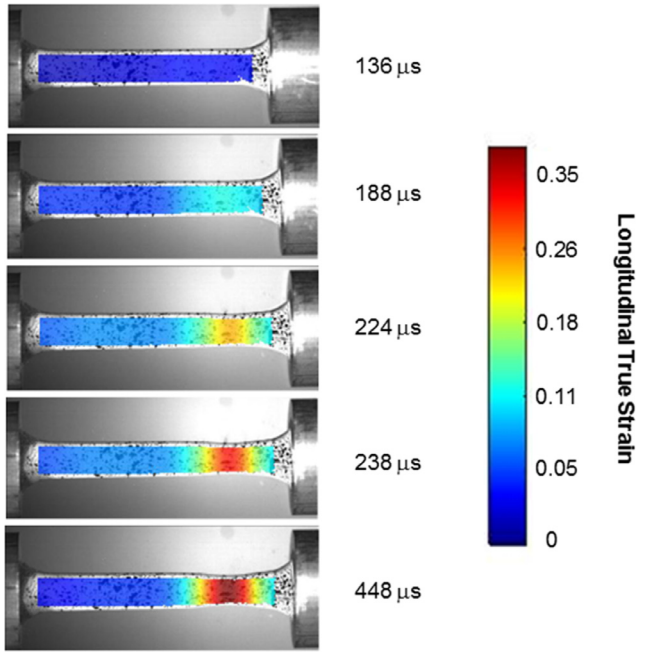

Fig. 9. DIC images for the dynamic tensile test L4_20_1 – showing stages in neck initiation and evolution.

specimen, up to fracture, which takes place at a final true strain of 80%.

3.2. Dynamic compression tests

In Fig. 6, two stress-strain curves are shown for PC, analyzed from two Kolsky-Bar tests, varying slightly in the impact velocity, thus the difference in their maximum strain. Two additional curves are shown for comparison, from the work of Mulliken and Boyce (2006) and from the work of Rittel and Levin, (1998). The agreement of our current results with the literature is good.

The observed peak flow stress upon yield is between 115 [MPa] to 125 [MPa] and the maximum measured true strain is 85%.

3.3. Dynamic tensile tests

A total of 10 tests were conducted on the Kolsky-Bar, summarized in Table 1. Specimens with various combinations of diameter and length were used to assess the effect of specimen geometry on the results. However, local deformation at the thread region was noticed for gauge diameters larger than 4 mm, therefore, the data from the tests with the larger diameters enabled limited data to account for.

The strain gauge signals from test L4_20_5 are shown in Fig. 7. Due to the low mechanical impedance of the polymer specimen, only a small part of the incident pulse is transmitted through the specimen, resulting in a very low amplitude of the transmitted signal. Yet, a sufficiently significant transmitted signal is still obtained to allow further analysis of the results. The transmitted signal shows an initial high spike referring to the axial inertia of the attached aluminum flange and momentum trap at the incident-bar end. The oscillations are the result of wave dispersion.

Fig. 8 shows records of the forces acting on both sides of the tensile specimen. F_{in} is calculated from the sum of the incident and reflected signals, resulting in a noisy result which was smoothed out for comparison with F_{out}. We believe these oscillations are a result of the initial gap upon mounting, between the specimen and the bars. This was demonstrated in Sarva and Boyce (2007), showing such oscillations when a small gap of 0.1–0.5 mm was present. This gap is a result of necessary manufacturing tolerances to ensure the assembly of the specimen in the bars. The high frequency noise was filtered to remove and maintain a reliable signal for analysis, as the material-related (constitutive) signal does not contain high frequency features.

In Fig. 8, we show that for a criterion of ~10% difference between the forces, equilibrium is reached after approximately 60 μs. From this point of equilibrium on, the determination of the stress, strain and strain-rate is straightforward using the standard Kolsky-Bar analysis.

Fig. 9 presents the stages of strain evolution, as recorded by the DIC analysis of the high speed camera pictures. Fig. 10 shows the strain history measured in the middle of the neck region in comparison with the averaged strain along the specimen gauge length. The differences, showing a factor of 3 between the average and local strains (0.13 compared with 0.38) demonstrate the necessity and advantage of *local measurements* to enable the material characterization at much larger strains.

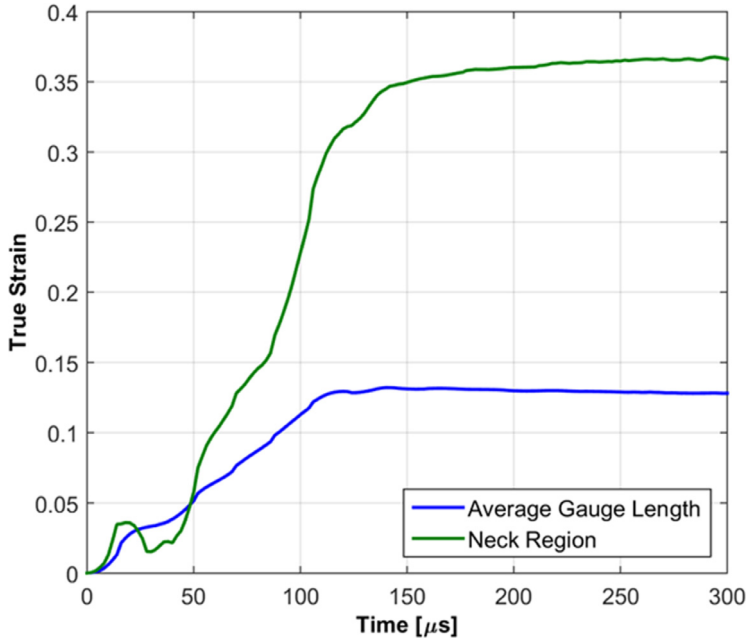

Fig. 10. Longitudinal true strain history in test L4_20_1, measured using DIC: at the neck location and the average strain along the specimen.

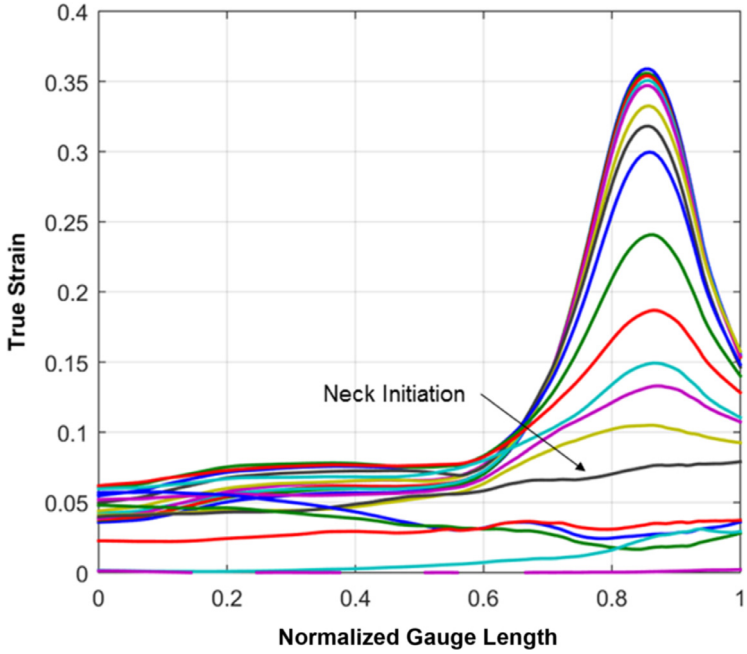

Fig. 11. Longitudinal true strain evolution along PC specimen L4-20-1 normalized gauge length (Time steps every 10 μs).

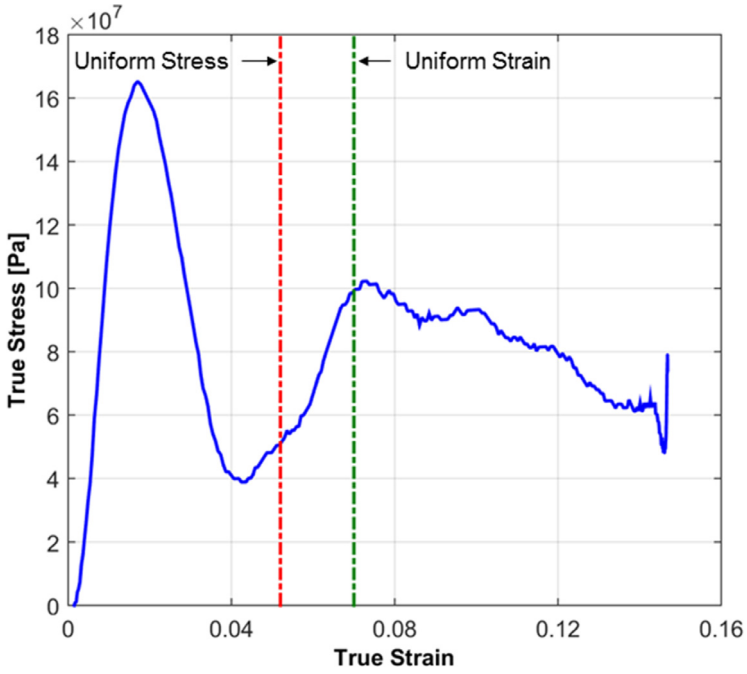

Fig. 12. True Stress-Strain curve of PC for dynamic tensile test L4_20_1, the curve is valid only between the two vertical dashed lines where both the stress and strain are homogenous.

The evolving strain distribution along the specimen is shown in Fig. 11, in time steps of 10 μs. The location of the neck initiation can be seen on the right side of the specimen with a value of ~7%, corresponding with the point in Fig. 11 , at which the two curves begin to separate.

The measured material response of PC for this experiment is shown in Fig. 12. This curve contains two limits, defining the range of validity for the standard Kolsky-bar analysis: from the equilibrium requirement we get the minimum strain, for which a uniform stress exists, and from the DIC measurements we get the maximum strain for which a uniform strain state exists, prior to localization. These limits define a very narrow range for a reliable analysis of the stress-strain curve, between 5% and 7%. In the next section, we will show that analysis within the neck region can enable the material characterization up to much higher strains. Furthermore, the use of simulations, implementing an inverse FE method and referring to the actual evolving stresses defuses the demand on uniformity of stresses and strains for a reliable and correct analysis.

4. Inverse finite element characterization

In the absence of equilibrium and a homogeneous state of stress and strain, all required for the classical Kolsky-bar analysis, we chose to focus on the material behavior within the neck. We found the

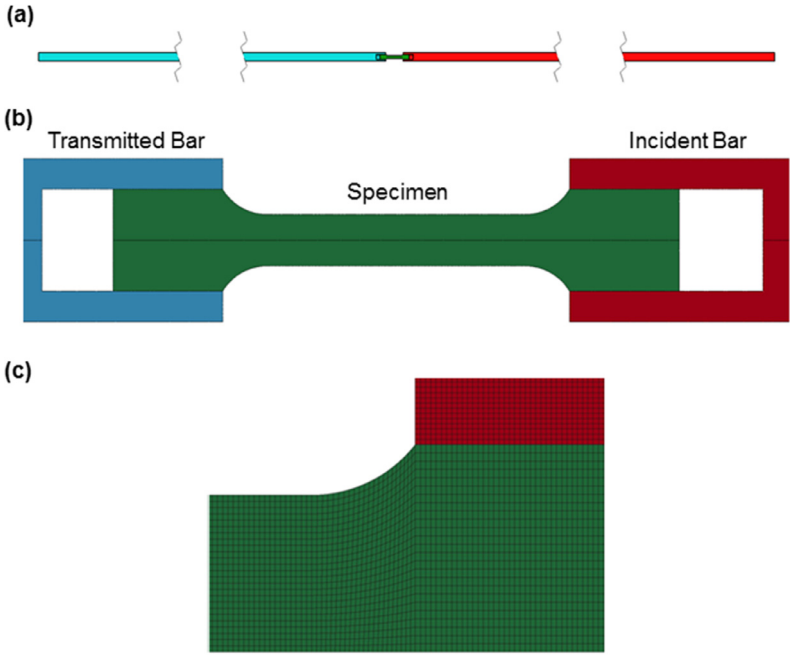

Fig. 13. Numerical simulation model (Ls-Dyna):(a) Full model of the Kolsky-bar apparatus, (b) Specimen mounting in the model (c) Zoom-in on the specimen mesh: shoulder, fillet and the gauge section.

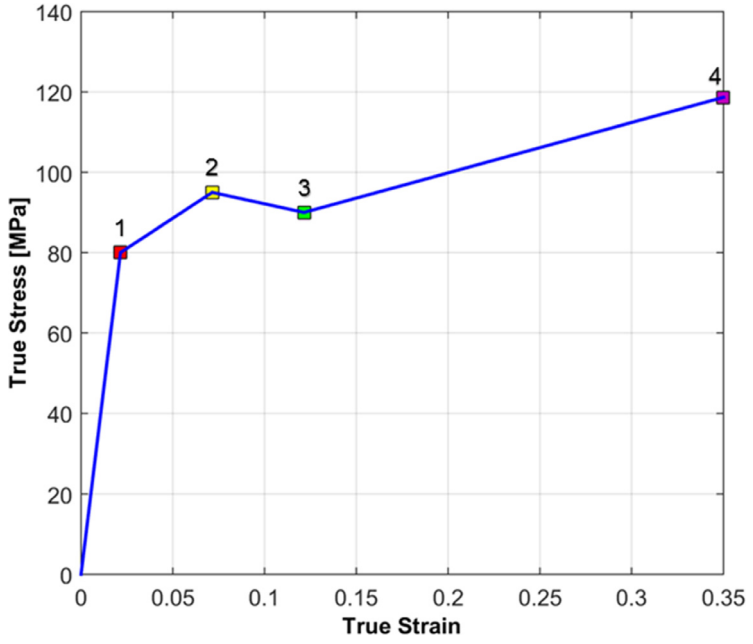

Fig. 14. The suggested 4-point material model for polycarbonate.

measurement within the neck region to carry much data and information, comparable with the numerical analysis. Furthermore, the material reaches much higher strains in the neck and a corresponding stress strain curve could thus be obtained in principle. We conducted numerical simulations with the commercial finite element package LS-Dyna (LS-DYNA, 2007), following an Inverse Finite Element identification procedure. The Inverse finite element (IFE) method is a numerical approach in which an optimal fit of the simulated data to the experimental data is sought. In general, this method can be used in order to find optimal values for any set of target parameters. Specifically, for the dynamic tensile test, we can assume a material model for the PC specimen and calibrate its values by best fitting as much data as possible from the test results. Our main guidelines for such a model were: (1) a simple model, using few model parameters as possible, (2) reflect the physics underlying the material's behavior. We used the experimentally measured velocity as an initial condition on the boundary, and the DIC strain measurements and strain gauges signals to compare with numerical gauges in the simulations. Comparable data are the strain history at the center of the neck region, the neck width, its position along the specimen and the bar strain gauge signals. The IFE method assumes that a good match between the simulation and the experimental results indicates that the material model describes well the material behavior of the specimen during the test. However, even though the comparison may show a good match, this does not guarantee a single unique material model. We try to address this possibility by trying to express as much physics as possible in the model behavior,

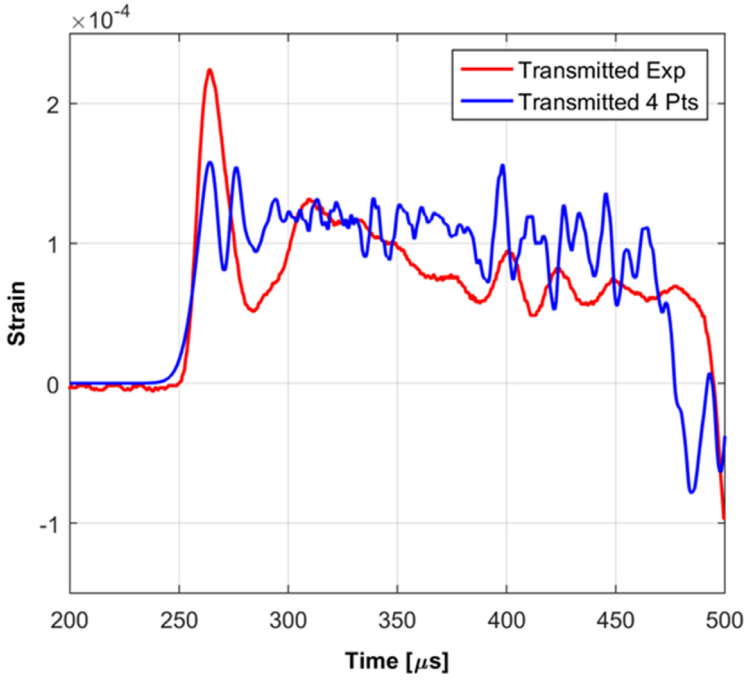

Fig. 15. Transmitted signal of test L4_20_1: comparison of the experimental transmitted signal and the calculated transmitted signal using the 4-point model.

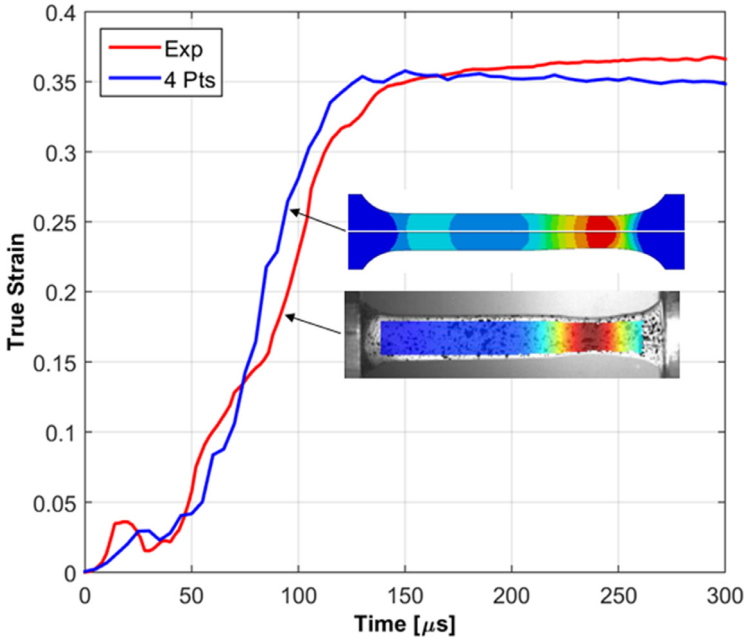

Fig. 16. True strain history in test L4_20_1 at the center of the neck: experimental measurement Vs simulation with 4-point model.

relating to as much possible data from the test.

The FE model includes an axi-symmetric representation of a direct Kolsky-bar apparatus. All calculations were performed with 2D Lagrangian axisymmetric elements. The element type used for all parts was a first order hexagonal element with 4 nodes and a single integration point. The specimen gauge section was meshed with a uniform mesh to avoid artificial localization stemming from the mesh topography. The characteristic mesh size along the specimen gauge was set to be 0.1 mm, while elements with characteristic length of 0.3 mm were used in the Kolsky tensile bars. The meshed model of the specimen mounted to the bars is shown in Fig. 13.

The tensile bars were considered to be purely elastic, therefore an elastic material model was used with an elastic module of E = 71.7 GPa. For the PC specimen, we adopted a simple phenomenological material model which takes into account the mechanisms we have observed in the quasi-static tensile tests and in the dynamic compression ones. We propose the following 4-point model, shown in Fig. 14.

The simple 4-point model follows the dominant material physics we identified from the dynamic compression tests:

(1) A linear elastic stage
(2) A hardening stage up to initial yield
(3) Softening due to the neck evolution
(4) Hardening referred to polymer-chain stretching

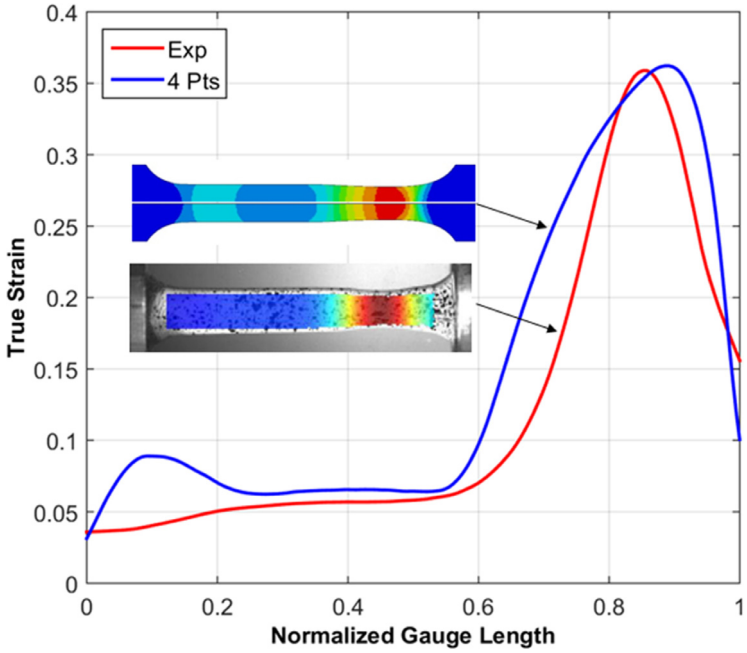

Fig. 17. Final strains in specimen L4_20_1: True strain distribution along normalized gauge length, DIC Measurement Vs simulation with 4-point model.

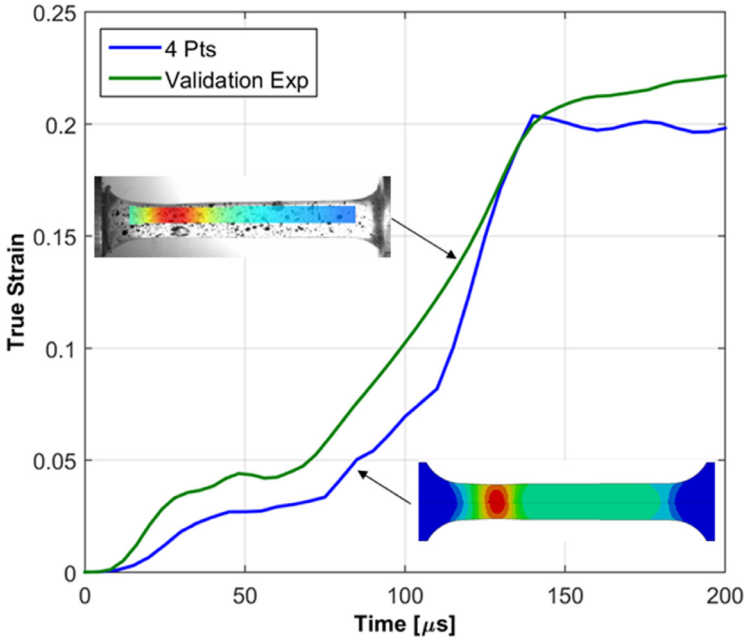

Fig. 18. True strain history in test L4_20_2 at the center of the neck: experimental DIC measurement Vs simulation with 4-point model.

The values of Pt. 1 and Pt. 2 are related to the elastic modulus and the neck initiation. The slope to point 1 is defined by the elastic modulus (3.7 GPa). For Point 2 we fixed the strain at which necking occurred to be 7%, as we found reproducible in our tests. The stress levels for point 1 and 2 were examined in the range of 80–100 MPa which matched our measurements and those in the literature (e.g, Mulliken and Boyce, 2006; Rittel and Levin, 1998). They were calibrated eventually with the corresponding values of 80 MPa and 95 MPa. The values of Pt. 3 and Pt. 4 control the softening stage, followed by a hardening phase. For these points, changes were examined moving both the strain and stress levels. These points were calibrated to match the neck location, neck width and final strain value. Their calibrated values are shown in Fig. 14. We further note that the calibrated piecewise linear model accounts effectively also for possible temperature effects (by plastic work), although they were not explicitly accounted for.

To examine the ability of this model, we calibrated the parameters to fit the results of one of the tests and then validated them for the other tests which varied in the total strain and also in the neck's location.

Fig. 15 shows the comparison between the simulated transmitted signal and the experimentally measured one for test L4_20_1. Examining the signal's average value, the comparison is reasonable, yet differences are evident, specifically not capturing the inertial peak. This is not surprising as the numerical model does not include the flange, directly impacted by the tubular impactor and not the momentum trap which both play the dominant role in the evolution of this inertial peak. Although these differences define the details in the transmitted signal, they are not essential for characterizing the properties of the specimen in the inverse FE method, which is based mainly on the direct DIC

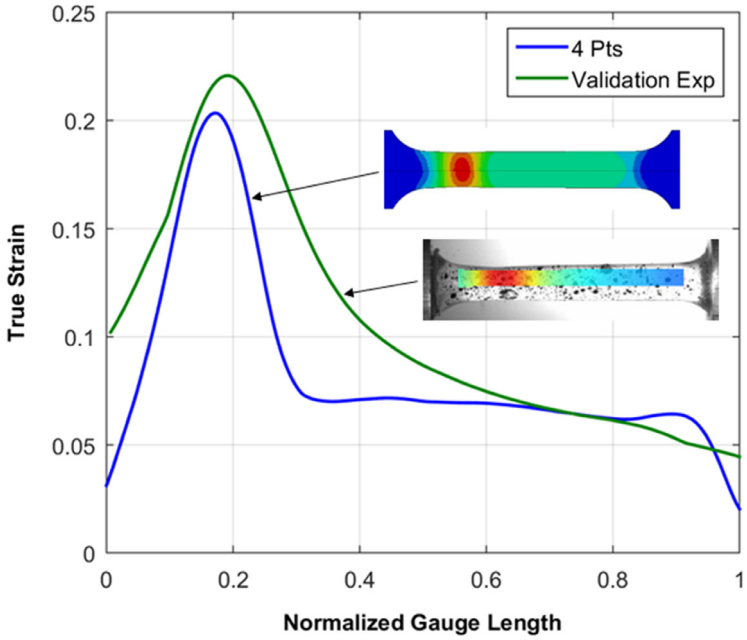

Fig. 19. Final strains in specimen L4_20_2: True strain distribution along the normalized gauge length, DIC measurement Vs simulation with 4-point model.

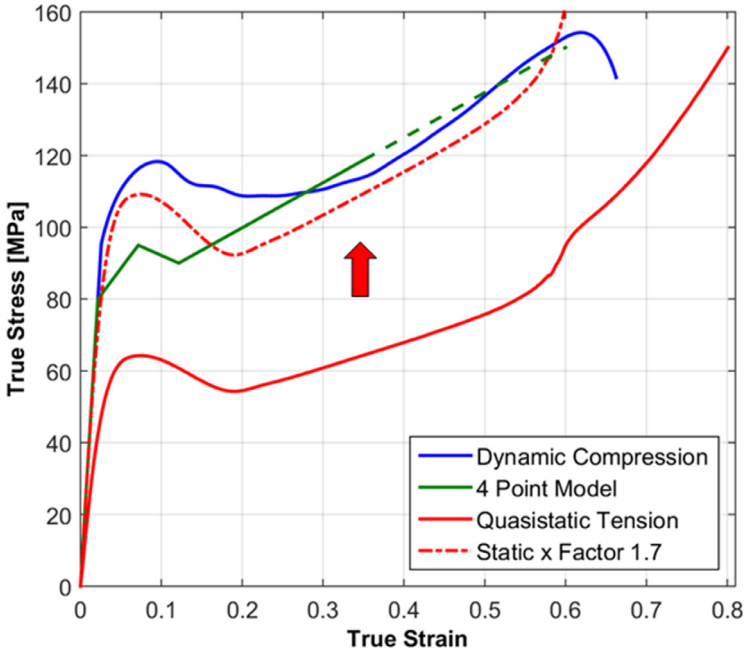

Fig. 20. Comparison between quasi-static tensile test, dynamic compression test and dynamic tensile test. The dotted line is the measured static stress-strain curve multiplied by a factor of 1.7.

measurements.

Figs. 16 and 17 show a very good construction of the neck formation (strain history), neck width and location along the specimen gauge for test L4_20_1. In the presented results, the specimen has undergone necking but did not reach failure. The comparisons in Fig. 17 and later in Fig. 19 are presented for the final strains of the specimen.

The next step was a validation of the proposed model based on additional dynamic tensile experiments. For this purpose, we chose an experiment in which the neck had formed on the opposite side compared with the previous test – test L4_20_2. In addition, the final strain value is significantly different between the two experiments.

As can be shown in Figs. 18 and 19, the 4 point model succeeds to replicate quite well this experiment in relation to all measurable data: the neck width and location and the final value of plastic strain. It could be noticed that the neck created in the experiment is somewhat wider than the simulated neck and the value of the maximum strain generated in the experiment is slightly higher. These differences may result from some variability in the properties of the polymer, as the model is not calibrated to fit best all the test result but rather calibrate it by one and examine its ability to reproduce the other results. All in all, a very satisfactory comparison is achieved, thereby validating the overall approached presented in this work.

5. Discussion

5.1. PC behavior–tension vs. Compression

Fig. 20 presents the material behavior in dynamic tension, dynamic compression and quasi-static tension. The green curve is the 4-point model, which represents the dynamic behavior under tension, and the dashed line is a linear extension of the curve beyond the actually measured strains.

Comparing the three curves we can notice the following:

1. PC can withstand higher stresses in compression than in tension by a factor of about 20%, as a result of its pressure sensitivity.
2. The strain rate sensitivity in tension is significant. The analyzed dynamic tensile-strength ($\sim$1000 s^{-1}) is higher by about 70% by comparison with the quasi-static one.
3. The analysis suggests a strong correlation between material behavior in dynamic and quasi-static tension. The red dashed curve in Fig. 20 illustrates the extent of this correlation by multiplying the quasi-static tensile curve by a factor of 1.7. One can see similarities in the 4-point curve and the multiplied quasi-static tensile curve: the behavior stages of softening after yield is reached, followed by a hardening stage. Specifically, the strain hardening inclination compares very nicely. This also suggests that all stages of material behavior show similar strain rate sensitivity.
4. Furthermore, the measured behavior under dynamic compression shows a very similar behavior to that obtained under dynamic tension, comparable to the 4-point model and the factored static curve.

The similarity between the strain hardening slopes in the dynamic tension and compression curves can be possibly explained by the same physical mechanism. Strain hardening is principally due to changes in chain orientation. While in tension, the chains are aligning parallel to the stretching direction in the cold drawn regions, in compression, the chains are aligning in the plane *perpendicular* to the compression axis, referring to the Poisson effect.

These suggested correlations could possibly facilitate the measurement of the dynamic strength of ductile polymers – to be extracted from quasi-static tension or dynamic compression measurements only, which are much easier and straightforward to conduct and analyze. Furthermore, these suggested relations between the tension-compression and quasi-static-dynamic behaviors could be further implemented in an extended material model, accounting for corresponding pressure/triaxiality and strain rate dependences.

6. Summary and conclusions

We presented an Inverse FE approach to measure and analyze the dynamic stress-strain behavior of polycarbonate, using the Kolsky-bar apparatus. To overcome the difficulties of the direct measurements of polymers under dynamic tension, namely the (dis)ability to reach equilibrium and the low transmitted signal, we used high speed photography with DIC measurements, and FE numerical simulations. The analysis focused on the evolution of strain within the neck, allowing to reach high strains. We suggested and calibrated a phenomenological 4-point model which follows the dominant physics ruling the polycarbonate tensile behavior, implementing it in a simple stress-strain curve. This approach was successful in reconstructing for various experiments the distribution of the longitudinal strains formed along the specimen and the characteristics of the necking, namely, the location of the neck and the large strains evolution.

We further examined the material's behavior also in quasi-static tension and dynamic compression and compared the material behavior under these different loadings. The comparison suggests a strong correlation between them, following quite similar stages of behavior.

From the results we obtained in this research and their analysis, we came to the following conclusions:

a) The FEM inverse method, based on the comparison with DIC measurements, was found to be effective in characterizing the dynamic tensile behavior of PC. Specifically, focusing within the neck region was found to be a key factor in order to explore the material behavior, even when equilibrium in the specimen is not existent.
b) Analysis of the neck allows reaching high strains due to the strain localization, while the entire specimen reaches much lower averaged strains.
c) The analysis suggests a strong correlation between PC's behavior in dynamic tension and quasi-static tension. The qualitative material behavior was similar for the two cases and by using a constant factor of 1.7, a good quantitative match between the two stress-strain curves was achieved.
d) The analysis suggests a strong correlation between PC's behavior in dynamic tension and dynamic compression. We suggest that strain hardening in dynamic compression could be explained as a hardening mechanism in tension - the same as in direct tension.
e) This suggested correlation could possibly facilitate the measurement of the dynamic strength of polymers – to be possibly extracted from dynamic compression or quasi-static tension measurements only.

References

ASTM Int., 2016. ASTM E8/E8M - standard test methods for tension testing of metallic materials. ASTM Int. 1–27. http://dx.doi.org/10.1520/E0008_E0008M-16A.

Bacon, C., 1998. An experimental method for considering dispersion and attenuation in a viscoelastic hopkinson bar. Exp. Mech. 38, 242–249. http://dx.doi.org/10.1177/001448519803800402.

Benatar, A., Rittel, D., Yarin, A.L., 2003. Theoretical and experimental analysis of longitudinal wave propagation in cylindrical viscoelastic rods. J. Mech. Phys. Solids. 51, 1413–1431. http://dx.doi.org/10.1016/S0022-5096(03)00056-5.

Blaber, J., Adair, B.S., Antoniou, A., 2015. Ncorr: open-source 2D DIC Matlab software. Exp. Mech. 1105–1122. http://dx.doi.org/10.1007/s11340-015-0009-1.

Bridgman, P.W., 1952. Studies in Large Plastic Flow and Fracture. McGraw-Hill, New York.

Cao, K., Wang, Y., Wang, Yu, 2014. Experimental investigation and modeling of the tension behavior of polycarbonate with temperature effects from low to high strain rates. Int. J. Sol. Struct. 51, 2539–2548.

Chen, M.C.W., Lu, F., 2002. Tension and compression tests of two polymers under quasi-static and dynamic loading. Polym. Test. 21, 113–121.

Foster, M., Love, B., Kaste, R., Moy, P., 2015. The rate dependent tensile response of polycarbonate and poly-methylmethacrylate. J. Dyn. Behav. Mater. 1, 162–175. http://dx.doi.org/10.1007/s40870-015-0020-8.

Gerlach, R., Sathianathan, S.K., Siviour, C., Petrinic, N., 2011. A novel method for pulse shaping of Split Hopkinson tensile bar signals. Int. J. Impact Eng. 38, 976–980. http://dx.doi.org/10.1016/j.ijimpeng.2011.08.007.

Gray III, G.T., Blumenthal, W.R., Trujillo, C.P., Carpenter II, R.W., 1997. Influence of temperature and strain rate on the mechanical behavior of adiprene ι-100. In: J. Phys. IV JP.

Harding, J., Wood, E.O., Campbell, J.D., 1960. Tensile testing of materials at impact rates of strain. J. Mech. Eng. Sci. 2, 88–96. http://dx.doi.org/10.1007/BF02326644.

Kolsky, H., 1949. An investigation of the mechanical properties of materials at very high rates of loading. Proc. Phys. Soc. Lond. B. 62, 676–700.

Koubaa, S., Othman, R., Zouari, B., El-Borgi, S., 2011. Finite-element analysis of errors on stress and strain measurements in dynamic tensile testing of low-ductile materials. Comput. Struct. 89, 78–90.

LS-DYNA, 2007. Keyword User's Manual. Livermore Softw. Technol. Corp.

Mirone, G., 2004. A new model for the elastoplastic characterization and the stress-strain determination on the necking section of a tensile specimen. Int. J. Solids Struct. 41, 3545–3564. http://dx.doi.org/10.1016/j.ijsolstr.2004.02.011.

Mirone, G., 2013. The dynamic effect of necking in Hopkinson bar tension tests. Mech. Mater. 58, 84–96. http://dx.doi.org/10.1016/j.mechmat.2012.11.006.

Mulliken, A.D., Boyce, M.C., 2004. Low to high strain rate deformation of amorphous polymers. In: Proc. 2004 SEM X Int. Congr. Expo. Exp. Appl. Mech. pp. 7–10.

Mulliken, A.D., Boyce, M.C., 2006. Mechanics of the rate-dependent elastic-plastic deformation of glassy polymers from low to high strain rates. Int. J. Solids Struct. 43, 1331–1356. http://dx.doi.org/10.1016/j.ijsolstr.2005.04.016.

Nie, X., Song, B., Ge, Y., Chen, W.W., Weerasooriya, T., 2009. Dynamic tensile testing of soft materials. Exp. Mech. 49, 451–458. http://dx.doi.org/10.1007/s11340-008-9133-5.

Richeton, J., Ahzi, S., Vecchio, K.S., Jiang, F.C., Adharapurapu, R.R., 2006. Influence of temperature and strain rate on the mechanical behavior of three amorphous polymers: characterization and modeling of the compressive yield stress. Int. J. Solids Struct. 43, 2318–2335. http://dx.doi.org/10.1016/j.ijsolstr.2005.06.040.

Rittel, D., Levin, R., 1998. Mode-mixity and dynamic failure mode transitions in

polycarbonate. Mech. Mater. 30, 197–216. http://dx.doi.org/10.1016/S0167-6636(98)00042-8.
Rotbaum, Y., Rittel, D., 2014. Is there an optimal gauge length for dynamic tensile specimens? Exp. Mech. 54, 1205–1214. http://dx.doi.org/10.1007/s11340-014-9889-8.
Sarva, S., Boyce, M., 2007. Mechanics of polycarbonate during high-rate tension. J. Mech. Mater. Struct. 2, 1853–1880. http://dx.doi.org/10.2140/jomms.2007.2.1853.
Sawas, O., Brar, N.S., Brockman, R.A., 1998. Dynamic characterization of compliant materials using an all-polymeric split Hopkinson bar. Exp. Mech. 38, 204–210. http://dx.doi.org/10.1007/BF02325744.
Subhash, G., Liu, Q., Gao, X.L., 2006. Quasistatic and high strain rate uniaxial compressive response of polymeric structural foams. Int. J. Impact Eng. 32, 1113–1126. http://dx.doi.org/10.1016/j.ijimpeng.2004.11.006.
Walley, S., Field, J., 1994. Strain rate sensitivity of polymers in compression from low to high rates. dymat. J. 1, 211–227.
Wang, L., Labibes, K., Azari, Z., Pluvinage, G., 1994. Generalization of split Hopkinson bar technique to use viscoelastic bars. Int. J. Impact Eng. 15, 669–686. http://dx.doi.org/10.1016/0734-743X(94)90166-I.
Zhao, H., Gary, G., 1995. A three dimensional analytical solution of the longitudinal wave propagation in an infinite linear viscoelastic cylindrical bar. Application to experimental techniques. J. Mech. Phys. Solids. 43, 1335–1348. http://dx.doi.org/10.1016/0022-5096(95)00030-M.